Appendix

Appendix Figures and Figure Legends

Appendix Tables

Table of contents:

Appendix Figure S1. eCDNs induces IL-6 production in macrophages 2
Appendix Figure S2. Internalization of eCDNs..... 3
Appendix Figure S3. eCDNs-induced innate immune activation requires STING..... 4
Appendix Figure S4. Cellular compartmentalization of eCDNs puncta..... 5
Appendix Figure S5. Diagram showing involvement of cGAS in sensing of eCDNs .. 6
Appendix Table S1. SAXS Data collection and derived parameters..... 7

Appendix Figures and Figure Legends

Appendix Figure S1

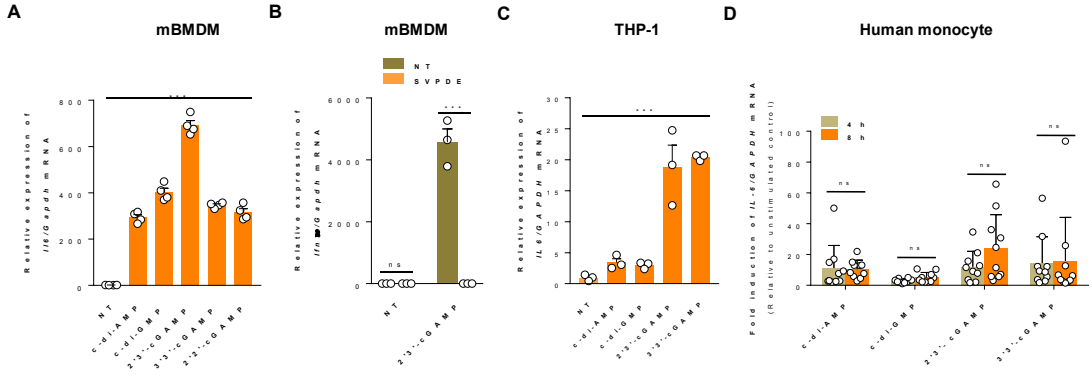

Appendix Figure S1. eCDNs induces IL-6 production in macrophages.

A qRT-PCR detection of IL-6 mRNA in mBMDMs stimulated with indicated eCDNs (5 μg/ml) for 4 h.

B qRT-PCR detection of IFNβ mRNA in mBMDMs stimulated with indicated ecGMAP (5 μg/ml) left pretreated or untreated with snake venom phosphodiesterase (SVPDE) for 4 h.

C qRT-PCR detection of IL-6 mRNA in THP-1 cells stimulated with indicated eCDNs (5 μg/ml) for 4 h.

D qRT-PCR detection of IL-6 mRNA in human PBMC-derived monocytes stimulated with indicated eCDNs (5 μg/ml) for 4 h or 8 h, respectively.

Data **(A-C)** are means+SD averaged from at least 3 independent experiments performed with biological triplicate and each symbol represents the mean of biological triplicates. Data in **(D)** are means+SD of 10 healthy donors, where each symbol represents one individual donor. One-way ANOVA followed by Dunnett's post hoc test **(A, C)** and Two-way ANOVA followed by Bonferroni's post hoc test **(B, D)** were used for statistical analysis, respectively. ***, $p<0.001$; ns, not significant.

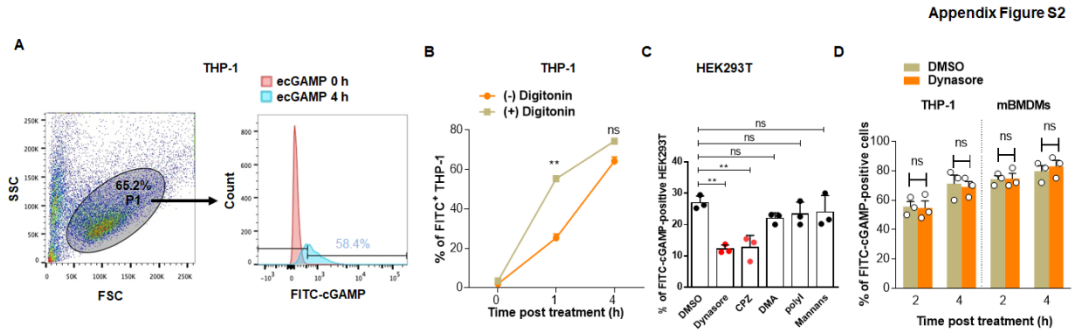

Appendix Figure S2. Internalization of eCDNs.

A Gating strategy for the FACS analysis of FITC$^+$ THP-1 cells. The live THP-1 cells were gated as P1. The frequency of FITC$^+$ THP-1 cells were calculated based on the control of unstimulated cells as shown on the right panel.

B Frequencies of FITC$^+$THP-1 cells stimulated with FITC-cGAMP (5 μg/ml) for indicated times in absence (–) or presence (+) of digitonin (10 μg/ml). Data are means+SD averaged from of 3 independent experiments performed with biological triplicates. Two-way ANOVA followed by Bonferroni's post hoc test was used for statistical analysis. $^{**}p<0.01$; ns, not significant.

C Frequencies of FITC$^+$ HEK293T cells stimulated with FITC-cGAMP for 1 h in presence of DMSO or indicated inhibitors including Dynasore (10 μM), chlorpromazine (CPZ, 10 μM), dimethylamiloride (DMA, 100 μM), polyinosinic acid (Poly I, 50 μg/ml) or mannans from *Sacharomyces cerevesiae* (Mannans, 1 mg/ml). Data are mean+SD and averaged from of 3 independent experiments performed with biological triplicates and each symbol represents the mean of biological triplicates. One-way ANOVA followed by Dunnett's post hoc test was used for statistical analysis, $^{**}p<0.01$; ns, not significant.

D Frequencies of FITC$^+$THP-1 cells or mBMDMs stimulated with FITC-icGAMP (0.1 μg/ml) for 4 h in the presence of DMSO or dynasore (10 μM). Data are means+SD averaged from of 3 independent experiments performed with biological triplicates. Two-way ANOVA followed by Bonferroni's post hoc test was used for statistical analysis. ns, not significant.

Appendix Figure S3

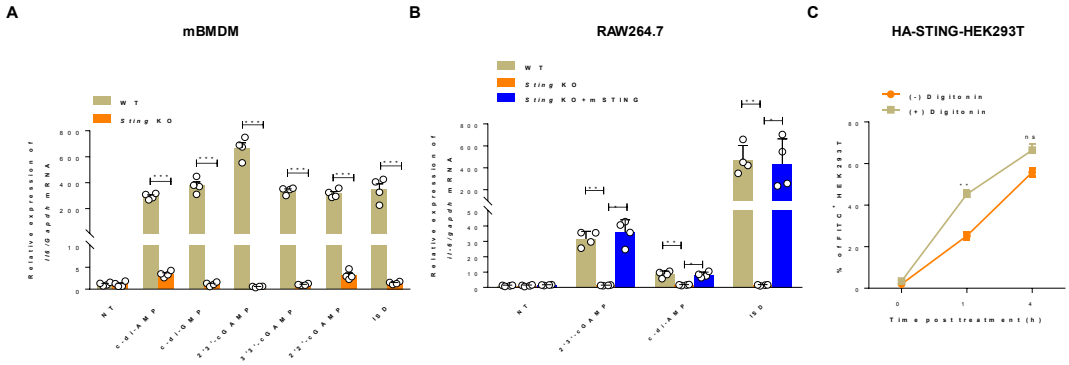

Appendix Figure S3. eCDNs-induced innate immune activation requires STING.

A qRT-PCR detection of IL-6 mRNA in WT and *sting*$^{-/-}$ mBMDMs stimulated with indicated eCDNs (5 μg/ml).

B qRT-PCR detection of IL-6 mRNA in WT, STING KO or STING KO complemented with mSTING (STING KO+mSTING) RAW264.7 cells stimulated with indicated eCDNs (5 μg/ml) or transfected with IFN stimulatory DNA (ISD).

C Frequencies of FITC^{+} HA-STING-HEK293T cells stimulated with FITC-cGAMP (5 μg/ml) for indicated times in the absence (–) or presence (+) of digitonin.

Data **(A-B)** are means+SD averaged from 4 independent experiments performed with biological triplicates, where each symbol represents the mean of biological triplicates. Data **(C)** are means±SD averaged from 3 independent experiments performed with biological triplicates. Two-way ANOVA followed by Bonferroni's post hoc test was used for statistical analysis. *, p<0.05; **p<0.01; ***, p<0.001.

Appendix Figure S4

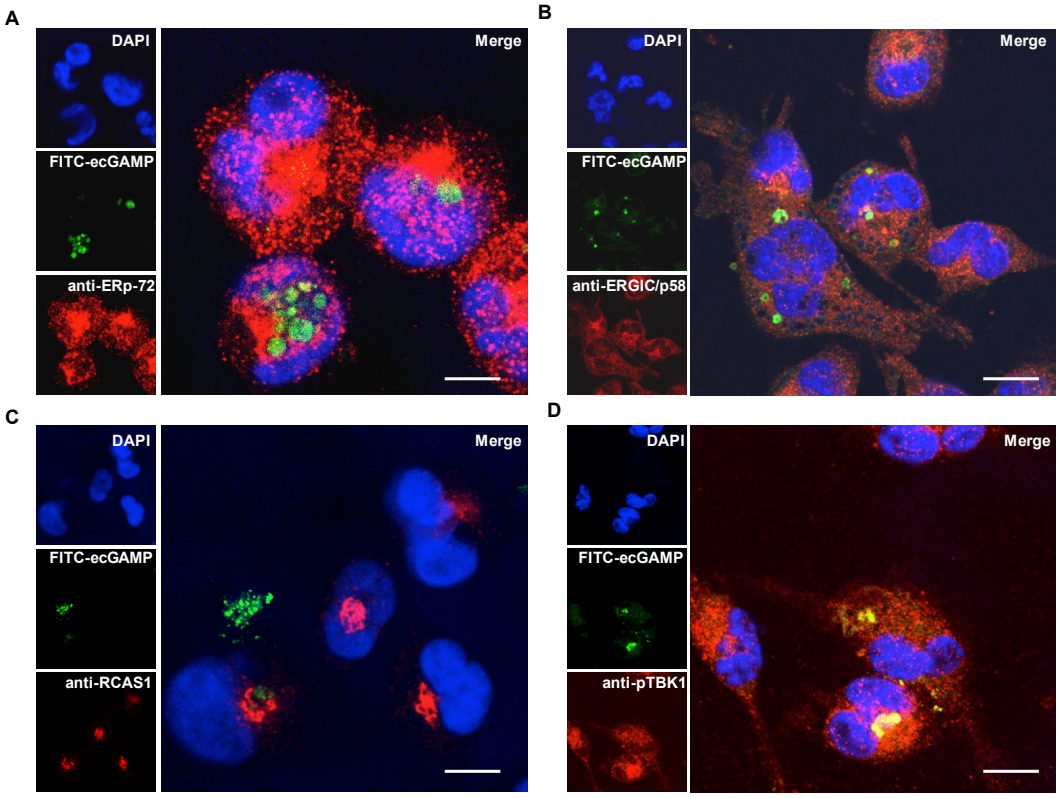

Appendix Figure S4. Cellular compartmentalization of eCDNs puncta. Immunostaining of ER (anti-ERp-72, red) **(A)**, ERGIC (anti-ERGIC/p58, red) **(B)**, Golgi (anti-RCAS1, red) **(C)** and phospho-TBK1 (anti-phospho-TBK1, red) **(D)** in THP-1 cells stimulated with FITC-ecGAMP (5 μg/ml, green) for 2 h, nucleus in blue (DAPI). Data are representative of at least 3 independent experiments. Scale bar, 10 μm.

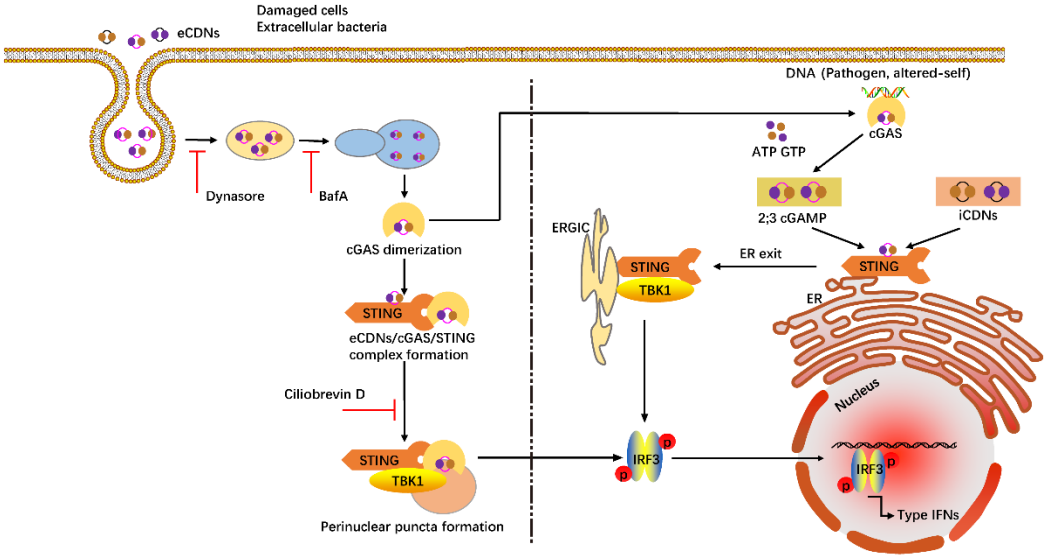

Appendix Figure S5. Diagram showing involvement of cGAS in sensing of eCDNs. The right panel depicts the DNA recognition by cGAS and the downstream events leading to type I IFN release. The left panel summarizes mechanisms governing eCDN sensing as indicated by current data. Clathrin-dependent endocytosis and endosome maturation are critical for sensing of eCDNs. Internalized CDNs bind cGAS directly, leading to its dimerization and promoting the formation of cGAS/STING complex. cGAS thus serves as a scaffolding protein and nucleates the formation of perinuclear signalosomes encompassing eCDNs/cGAS/STING which enables STING activation. Interestingly, eCDNs-induced dimerization of cGAS facilitates DNA sensing by cGAS.

Appendix Table S1. SAXS Data collection and derived parameters

Data collection parameters	cGAS	cGAS with 2′3′-cGAMP
Instrument	P12 at EMBL/DESY, storage ring PETRA III, Germany	
Beam geometry	0.2 × 0.12 mm2	
Wavelength (Å)	1.24	
s-range (Å−1)	0.002 – 0.47	
Exposure time (s)	3600 × 1	
Temperature (K)	283	
Structural parameters		
I(0) (arbitrary units) (from P(r))	2237.0 ± 22.4	2559.0 ± 25.6
Rg (from P(r)) (Å)	33.8 ± 1.7	41.2 ± 2.1
I(0) (arbitrary units) (from Guinier)	2166.9 ± 18.2	2543.39 ± 10.14
Rg (Å) (from Guinier)	31.4 ± 1.4	39.4 ± 0.9
Dmax (Å)	127.0 ± 6.0	141.1 ± 7.1
Porod volume (103 Å) 3	110.13	126.9
Ab initio model resolution (Å)	29 ± 2	25 ± 2

Molecular mass determination		
MMPOROD (from Porod volume) (kDa)	64.7 ± 6.5	74.7 ± 13
MMDAM (from bead model, kDa)	77 ± 10	98 ± 15
Calculated monomeric MM from sequence (kDa)	58.8	58.8
Software employed		
Primary data reduction	Automated radial averaging	
Data processing	PRIMUS	
Ab initio analysis	DAMMIF	DAMMIF
Validation and averaging	SASRES, DAMAVER	SASRES, DAMAVER
Modelling and flexibility analysis	EOM	EOM